Supporting Information

High entropy oxides as photocatalysts for organic conversion

Mingjin Li, [ab] Shuxing Mei, [c] Yong Zheng, [*ab] Long Wang [*ab] and Liqun Ye [*ab]

[a] College of Materials and Chemical Engineering, Key Laboratory of Inorganic Nonmetallic Crystalline and Energy Conversion Materials, China Three Gorges University, Yichang, 443002 (China)
[b] Hubei Three Gorges Laboratory, Yichang, 443007 (China)
[c] State Key Laboratory of Heavy Oil Processing at Karamay, China University of Petroleum-Beijing at Karamay, Karamay, 834000 (China)
E-mail: lqye@ctgu.edu.cn; wanglongchem@ctgu.edu.cn; zhengyong@ctgu.edu.cn

Contents

General Information

All raw materials and reagents are purchased from MACKLIN and HEOWNS Chemical Company, and the reagents are used without further purification, unless otherwise specified. The reaction products were monitored by thin layer chromatography (TLC) and purified by silica gel column chromatography (300~400 mesh). The liquid nuclear magnetic resonance spectrum (1H) was recorded on a 400 MHz NMR spectrometer (CDCl3 or d6-DMSO as solvent). The unit is ppm, and the internal standard is tetramethylsilane (TMS). This abbreviation is used to describe appropriate peak splitting patterns: s = singlet, d = bimodal, t = tristate, m = polymorphic. The coupling constant (J) is expressed in Hertz (Hz). The photo reactor is a 24 W blue light reactor of GeAo chemistry, with 24 1 W blue LEDs in series, wavelength: 455-470nm.

Results and Discussion

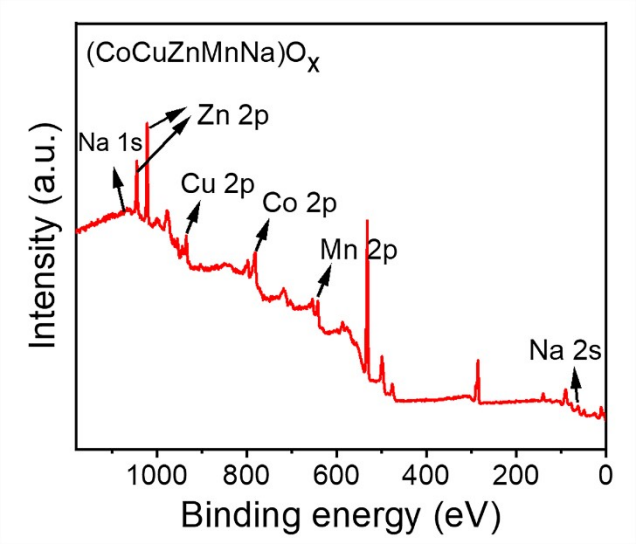

Fig. S1. Survey XPS spectrum of HEOs.

In addition, the UV visible diffuse reflectance absorption spectrum of HEOs shows a wide visible absorption range of up to 520 nm. Due to the grayish brown color of the HEOs, the material absorbs light from 500 to 700 nm (Fig. S2a). By using the Tauc plot, the optical band gap of HEOs was calculated to be 2.54 eV. As further support, the photocurrent response was recorded (Fig. S2b). When light is turned on, the photocurrent density of HEOs exhibits an enhanced response, indicating that HEOs exhibit advantages in photogenerated electron-hole separation and transmission efficiency. To determine their electronic band structure, Mott-Schottky measurements were performed on HEOs at three different frequencies of 200, 500, and 1000 Hz (Fig. S2c). The positive slope of the obtained C^{-2} value implies the characteristics of typical n-type semiconductors. Its flat charged potential is

extrapolated to -0.40 V vs. Ag/AgCl, which is more negative than the potential of O_2 to superoxide radical (-0.33 V vs NHE).

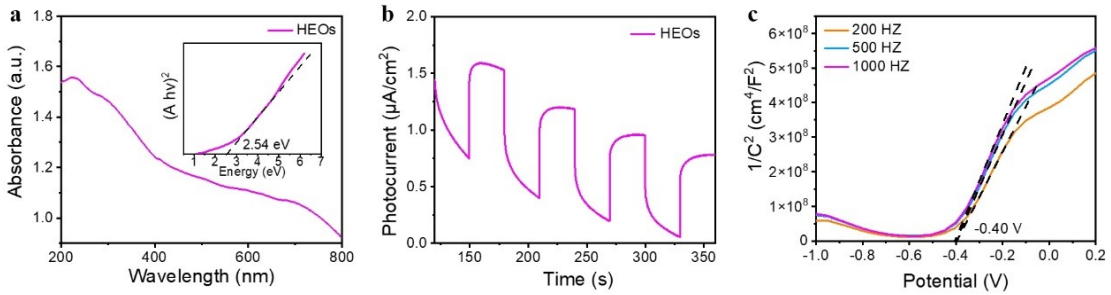

Fig. S2. Photoelectrochemical property. (a) Solid state UV-vis diffuse reflectance spectra, inset: Tauc plot of the HEOs. (b) Mott−Schottky plots of the HEOs. (c) Photocurrent responses spectra of the HEOs.

Photocurrent measurements showed a significant increase of photocurrent intensity of HEOs, indicating an enhanced photogenerated charge separation and electron transport than the control sample (Figure S3a). EIS revealed that the arc radius of HEOs was smaller than that of the control sample, reflecting lesser charge transfer resistances (Figure S3b).

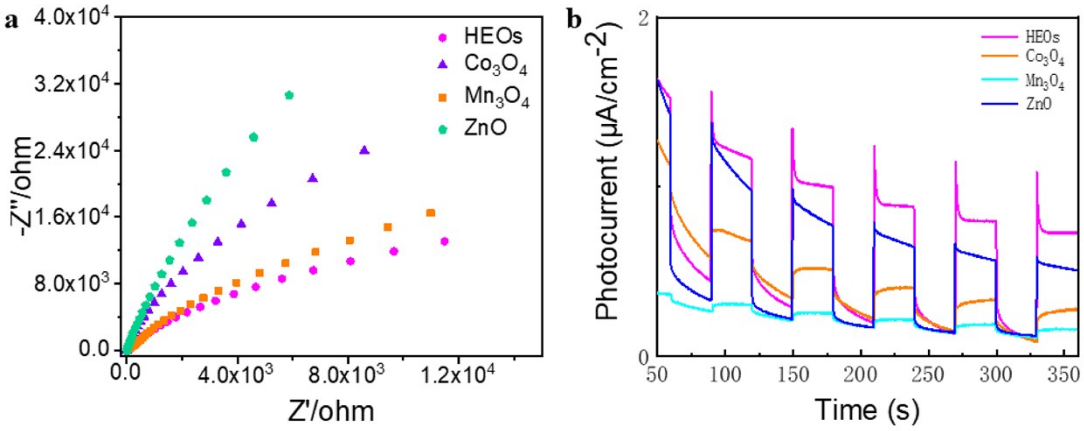

Fig. S3. (a) Impedance and (b) photocurrent diagrams of HEOs and Control Samples.

Oxidative coupling reaction of thiophenol in reaction 1 (Table S1). Firstly, in the solvent screening experiment. From Entry 1 to Entry 6, it can be seen that acetonitrile is the optimal solvent under the given conditions (Table S1, Entry 1). Then, screen the amount of catalyst used, it was not observed that increasing the amount of catalyst appropriately can further improve the yield (Table S1, Entry 7). Subsequently, it can be seen from Entry 8 that the high entropy oxide catalyst is important for the reaction. When the reaction lasted for 24 hours, the yield did not increase significantly (Table S1, Entries 9-11). The following research found that the occurrence of the experiment is also sensitive to light. Under dark light conditions, the yield is low (Table S1, Entry 12), indicating that light is also an important condition for the reaction. Under different light sources, the reaction will also occur, but blue light is the best light source for the reaction (Table S1, Entries 13 and 14). Under nitrogen atmosphere, the yield of the reaction system is only 27%, indicating that oxygen is required to participate in the reaction (Table S1, Entry 15). Finally, we conducted

a catalyst control experiment. The use of ZnO, Co_3O_4, and Mn_3O_4 photocatalysts in the experiment resulted in low yields (16%, 37%, and 24%) or almost no catalytic activity (Table S1, entries 16, 17, and 18). This indicates that synergy plays a major role. From the above experiments, it can be concluded that under standard conditions, HEOs play an important role in the reaction and are a good photocatalyst.

Table S1 Optimization of the reaction conditions for the oxidation of thiols to disulfides.[a]

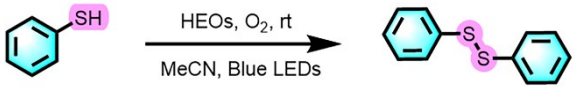

Entry	Solvent	Catalyst (mg)	Time (h)	Yield[b] (%)	Selective (%)
1	MeCN	HEOs (5 mg)	12	88	99
2	MeOH	HEOs (5 mg)	12	46	99
3	EtOH	HEOs (5 mg)	12	19	99
4	THF	HEOs (5 mg)	12	33	99
5	Acetone	HEOs (5 mg)	12	38	99
6	AcOEt	HEOs (5 mg)	12	54	99
7	MeCN	HEOs (10 mg)	12	89	99
8[c]	MeCN	0	12	11	99
9	MeCN	HEOs (5 mg)	1	46	99
10	MeCN	HEOs (5 mg)	6	64	99
11	MeCN	HEOs (5 mg)	24	90	99
12[d]	MeCN	HEOs (5 mg)	12	39	99
13[e]	MeCN	HEOs (5 mg)	12	80	99
14[f]	MeCN	HEOs (5 mg)	12	73	99
15[g]	MeCN	HEOs (5 mg)	12	27	99
16	MeCN	ZnO (5 mg)	12	16	98
17	MeCN	Co_3O_4 (5 mg)	12	37	98
18	MeCN	Mn_3O_4 (5 mg)	12	24	98

[a] Standard condition:Ar-SH (0.5 mmol), HEOs (5 mg), MeCN (2 mL), O_2, Blue LEDs (30 mW/cm^2), room temperature. [b] Yield was determined column separation. [c] No catalyst. [d] No light. [e] White LEDs. [f] Green LEDs. [g] Nitrogen atmosphere.

When no catalyst is added to the system, the yield is low, indicating that the reaction requires the participation of catalyst (Table S2, Entry 8). Then, through the catalyst dosage control experiment, it was found that when the catalyst dosage was increased, the yield did not significantly increase (Table S2, Entry 9). Afterwards, the high yield rate was found in the light source control experiment for all three types of light sources, but we still chose a 24 W blue LED light for the experiment (Table S2, Entries 10 and 11). We also tried to complete this experiment in water, and found that the yield was very low, probably because the raw materials could not be well dissolved in water, which led to the system could not fully react (Table S2, Entry 12). The system is difficult to convert in a nitrogen environment (Table S2, Entry 13). Finally, using ZnO synthesized by the same method to catalyze the reaction, ZnO has lower catalytic performance compared to high entropy oxides (Table S2, item 14). Similarly, the catalytic efficiency of Co_3O_4 and Mn_3O_4 is not ideal (Table S2, items 15 and 16), this fully confirms that the synergistic effect between various metals in high entropy oxides produces an effect of one plus one greater than two.

Table S2 Optimization of the reaction conditions.[a]

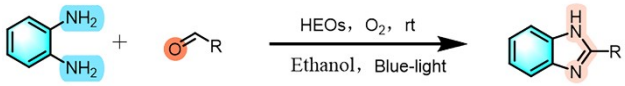

Entry	Solvent	Catalyst (mg)	Time (h)	Yield[b] (%)	Selective (%)
1	Ethanol	HEOs (5 mg)	1	91	98
2	MeOH	HEOs (5 mg)	1	48	98
3	DMF	HEOs (5 mg)	1	Trace	-
4	THF	HEOs (5 mg)	1	Trace	-
5	Acetone	HEOs (5 mg)	1	46	98
6	AcOEt	HEOs (5 mg)	1	Trace	-
7	MeCN	HEOs (5 mg)	1	Trace	-
8[c]	Ethanol	0	1	24	98
9[d]	Ethanol	HEOs (10 mg)	1	92	98
10[e]	Ethanol	HEOs (5 mg)	1	52	98
11[f]	Ethanol	HEOs (5 mg)	1	81	98
12[g]	Ethanol	HEOs (5 mg)	1	36	98
13[h]	Ethanol	HEOs (5 mg)	1	Trace	-
14	Ethanol	ZnO (5 mg)	1	65	97
15	Ethanol	Co_3O_4 (5 mg)	1	49	96
16	Ethanol	Mn_3O_4 (5 mg)	1	47	97

[a] Standard condition: o-phenylenediamine (0.5 mmol), benzaldehyde (0.5 mmol), HEOs (5 mg), Blue LEDs (30 mW/cm^2), O_2, room temperature, air. [b] Yield was determined column separation. [c] No catalyst. [d] 2 equivalen catalyst. [e] Green light. [f] white light. [g] Water as solvent. [h] Nitrogen atmosphere.

In order to study the mechanism of photocatalytic selective oxidation and conversion of HEOs, we conducted a series of quenching experiments using different scavengers (Fig. S4a). When 2,2,6,6-tetramethylpiperidine-1-oxyl (TEMPO, the scavenger of $^1O_2$) and *p*-benzoquinone (*p*-BQ, the $O_2^{\bullet-}$ scavenger) are added to the photocatalytic systems of **Reaction I** and **Reaction II**, respectively. The experimental results showed that System I achieved yields of 5% and 37% respectively,[1] while System II achieved yields of 16% and 11% respectively,[2] both lower than the yields under standard conditions. Therefore, it can be inferred that the reactive oxygen species (ROS) in the system are $O_2^{\bullet-}$ and $^1O_2$.[3]

To further confirm the production of $O_2^{\bullet-}$ and $^1O_2$ during photocatalytic oxidation, in situ electron spin resonance (ESR) was performed using 2,2,6,6-tetramethylpiperidine (TEMP) and 5,5-dimethyl-1-pyrroline N-oxide (DMPO) as capture agents under O_2 atmosphere, and 5 mg of HEOs were added to provide direct evidence (Fig. S4b). Different ESR signals irradiated by O_2 were detected, verifying the generation of $O_2^{\bullet-}$ captured by DMPO under visible light. Similarly, when TEMP was added, the 1:1:1 triplet state response signal characteristics of TEMPO were observed, indicating the generation of $^1O_2$.

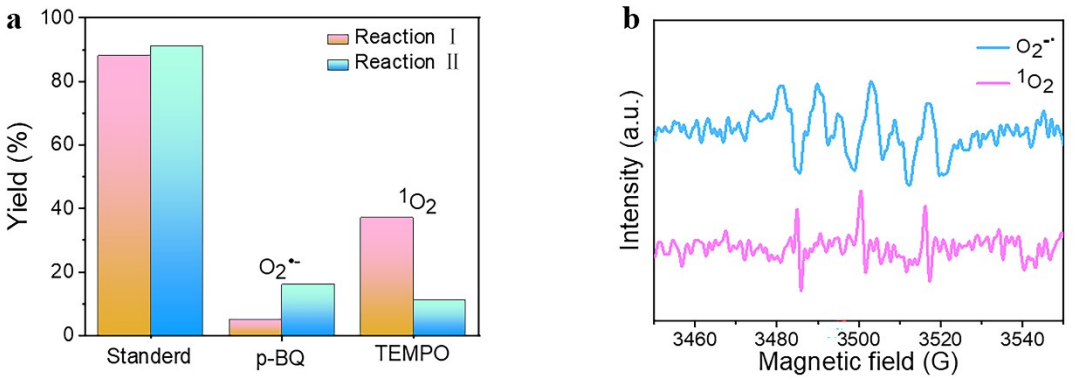

Fig. S4 (a) Effect of scavengers on photocatalytic oxidation conversion reaction. (b) In situ EPR signals labeled by DMPO for $O_2^{\bullet-}$ in dispersions, and in situ EPR signals labeled by TEMP for $^1O_2$ in dispersions.

^{1}H NMR and^{13}C NMR spectra and analysis of products[3, 4].

1,2-diphenyldisulfane

^{1}H NMR (400 MHz, $CDCl_3$) δ 7.53 – 7.46 (m, 4H), 7.30 (dd, *J* = 10.3, 4.7 Hz, 4H), 7.22 (t, *J* = 7.3 Hz, 2H).

^{13}C NMR (101 MHz, $CDCl_3$) δ 137.05, 129.07, 127.54, 127.17.

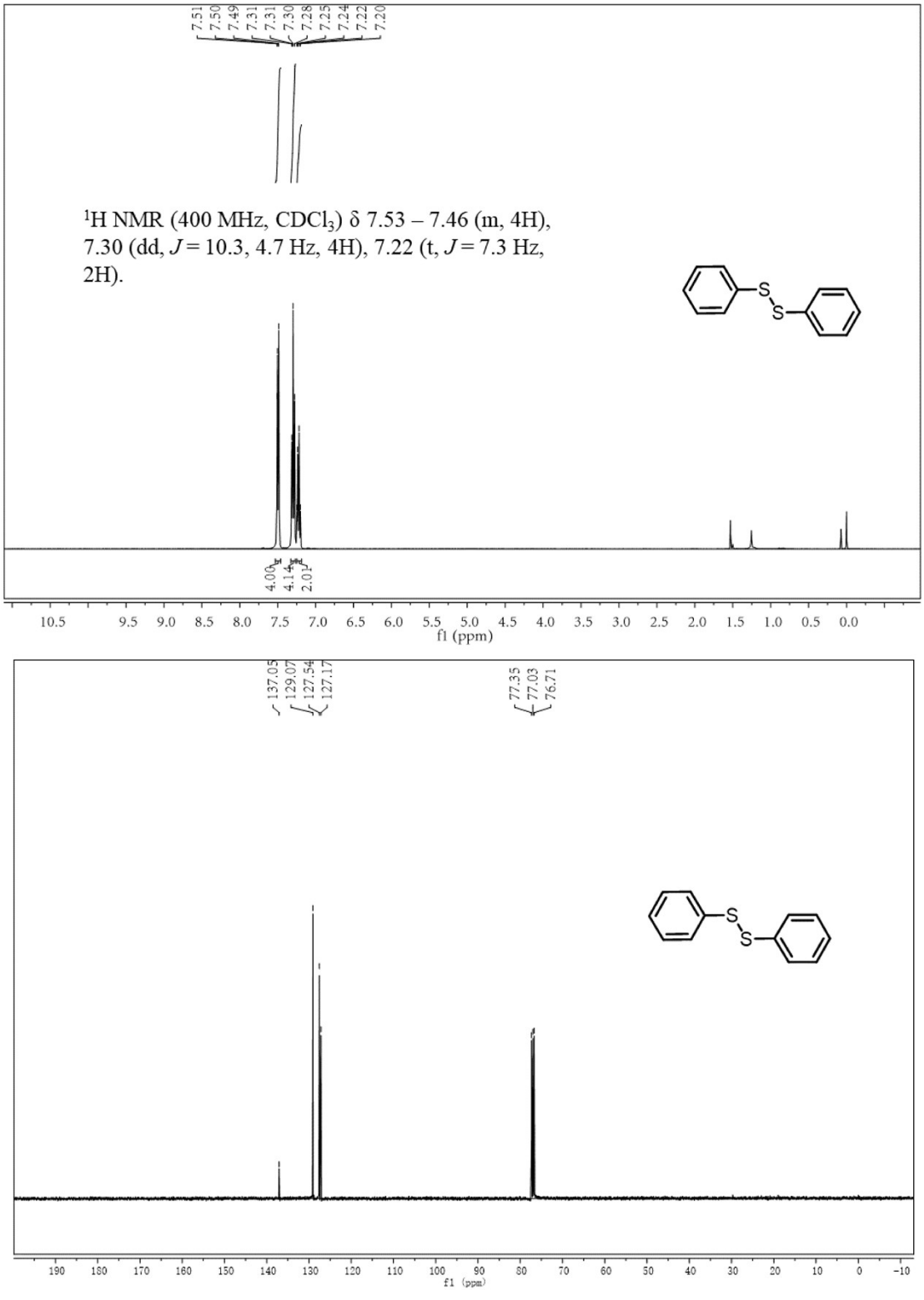

Fig. S5. ^{1}H NMR and^{13}C NMR spectrum of Diphenyl disulfide.

1,2-di(pyridin-2-yl)disulfane

^{1}H NMR (400 MHz, $CDCl_3$) δ 8.47 (d, J = 4.3 Hz, 1H), 7.83 – 7.44 (m, 2H), 7.11 (ddd, J = 6.6, 4.9, 2.0 Hz, 1H).

^{13}C NMR (101 MHz, $CDCl_3$) δ 158.96, 149.56, 137.38, 121.10, 119.69.

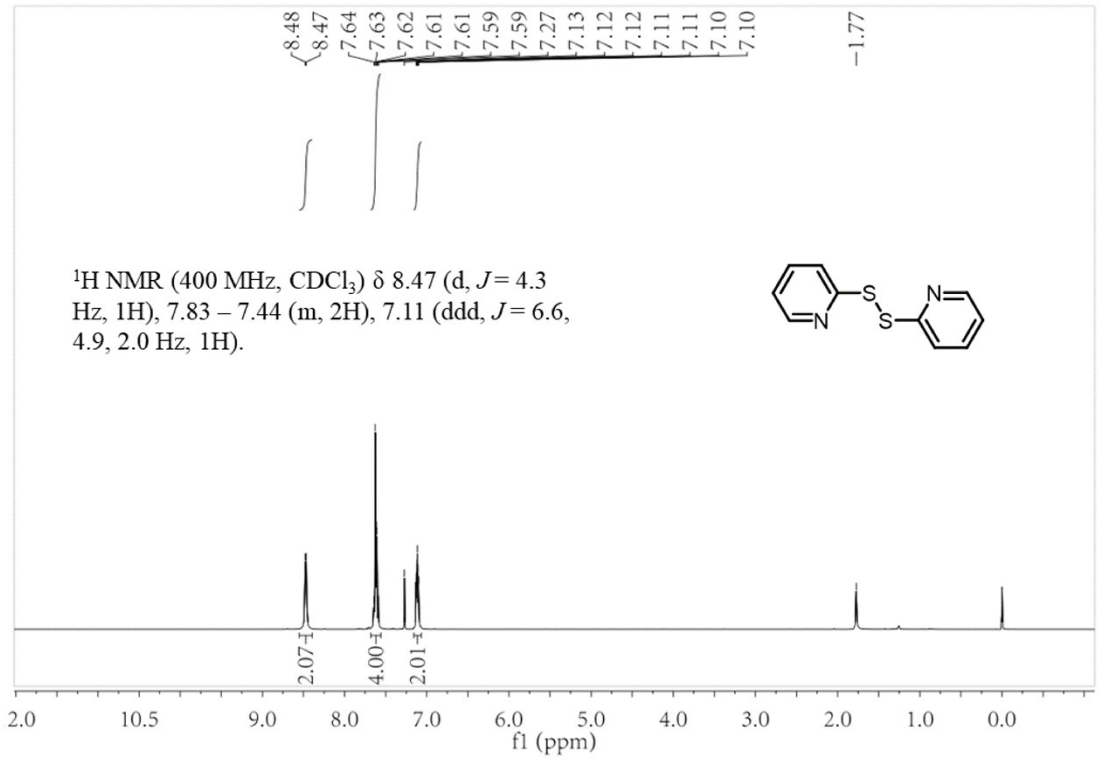

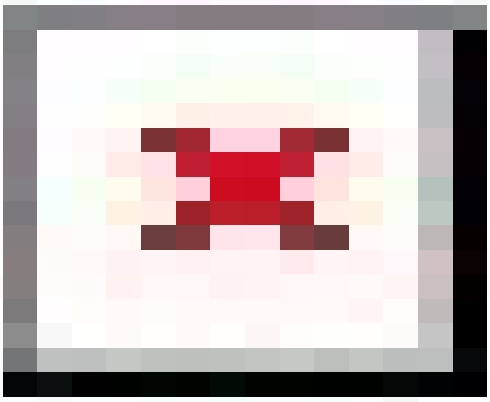

Fig. S6. ^{1}H NMR and ^{13}C NMRspectrum of 2, 2 '- dipyridyl disulfide.

1,2-bis(4-bromophenyl)disulfane

^{1}H NMR (400 MHz, $CDCl_3$) δ 7.45 – 7.40 (m, 4H), 7.38 – 7.29 (m, 4H).

^{13}C NMR (101 MHz, $CDCl_3$) δ 135.75, 132.23, 129.42, 121.56.

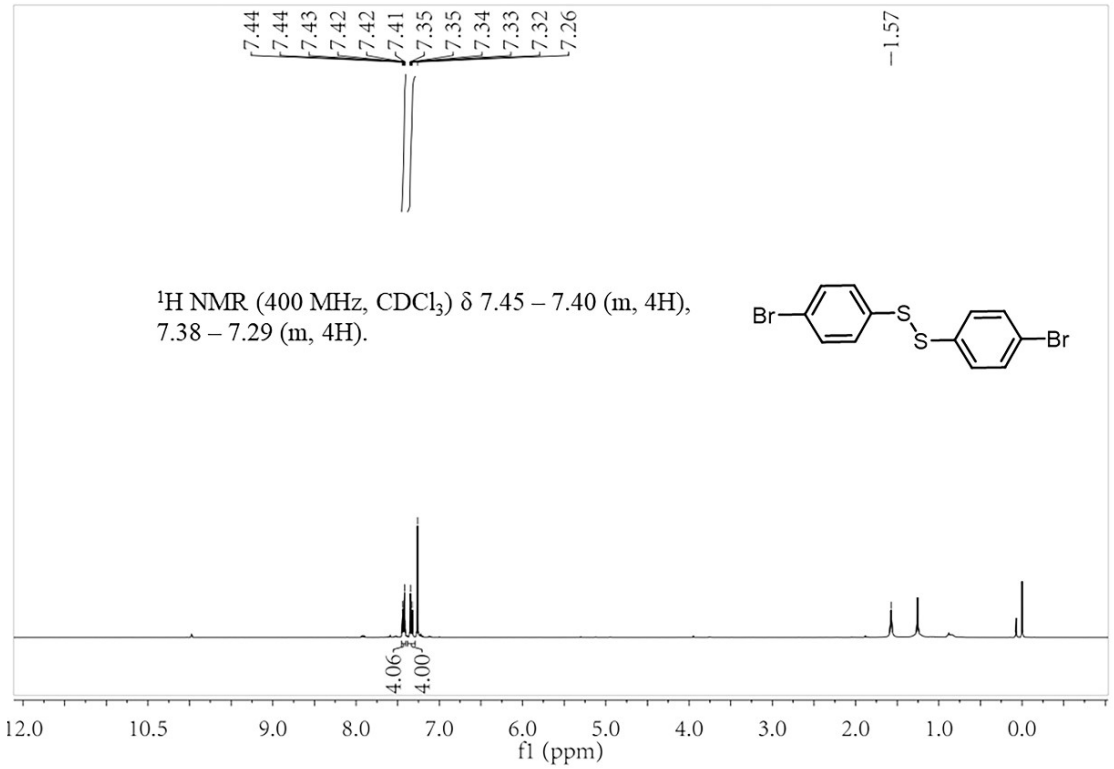

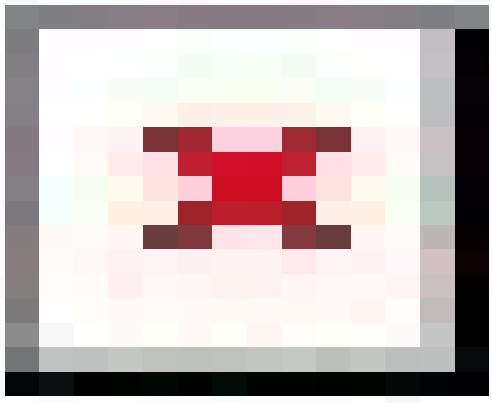

Fig. S7. ^{1}H NMR and ^{13}C NMR spectrum of 4,4 '- Dibromodiphenyl disulfide.

2,2 '- Dibromodiphenyl disulfide

^{1}H NMR (400 MHz, $CDCl_3$) δ 7.53 (dd, *J* = 8.0, 1.3 Hz, 4H), 7.29 – 7.22 (m, 2H), 7.07 (td, *J* = 7.7, 1.5 Hz, 2H).

^{13}C NMR (101 MHz, $CDCl_3$) δ 136.18, 132.94, 128.22, 127.95, 126.99, 121.10.

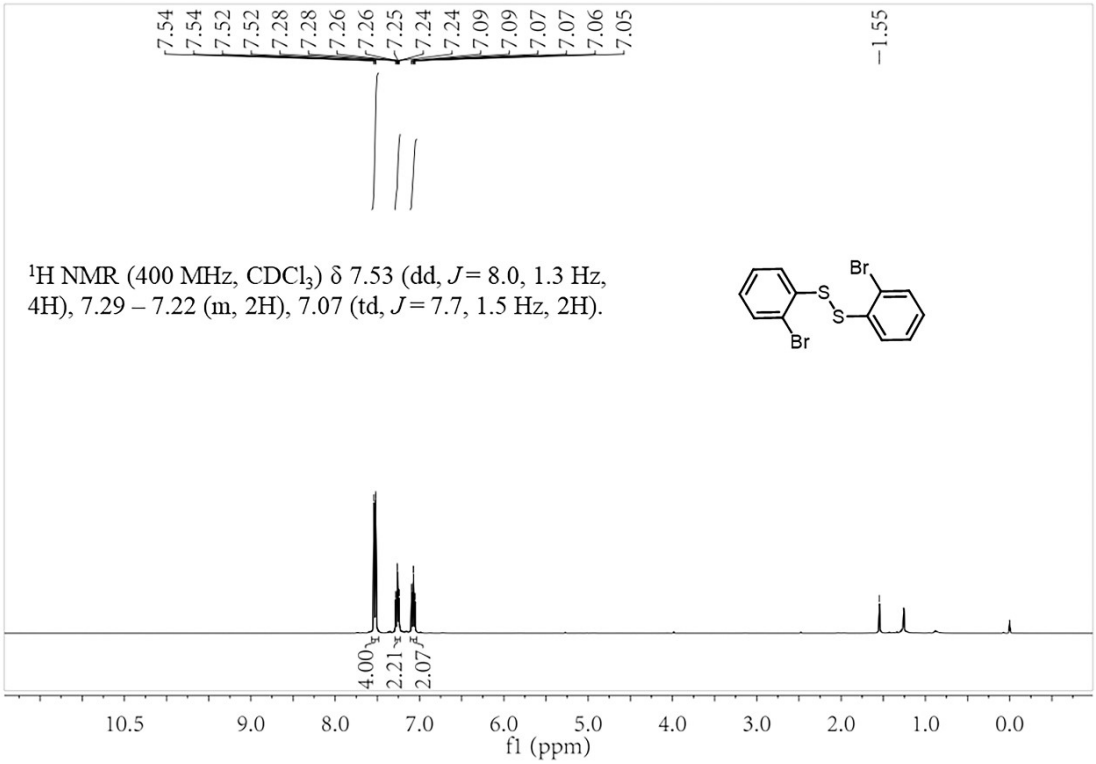

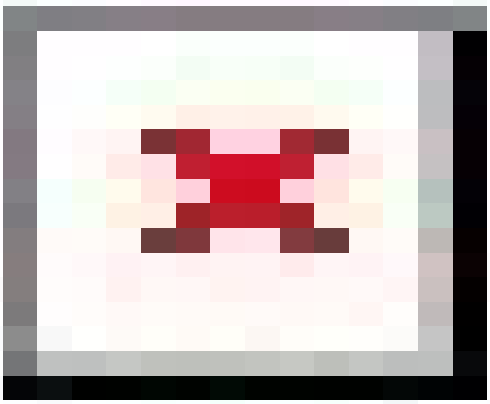

Fig. S8. ^{1}H NMR and ^{13}C NMR spectrum of 2,2 '- Dibromodiphenyl disulfide.

1,2-bis(4-chlorophenyl)disulfane

^{1}H NMR (400 MHz, DMSO) δ 7.57 – 7.51 (m, 4H), 7.49 – 7.44 (m, 4H).

^{13}C NMR (101 MHz, $CDCl_3$) δ 135.17, 133.68, 129.37, 129.33.

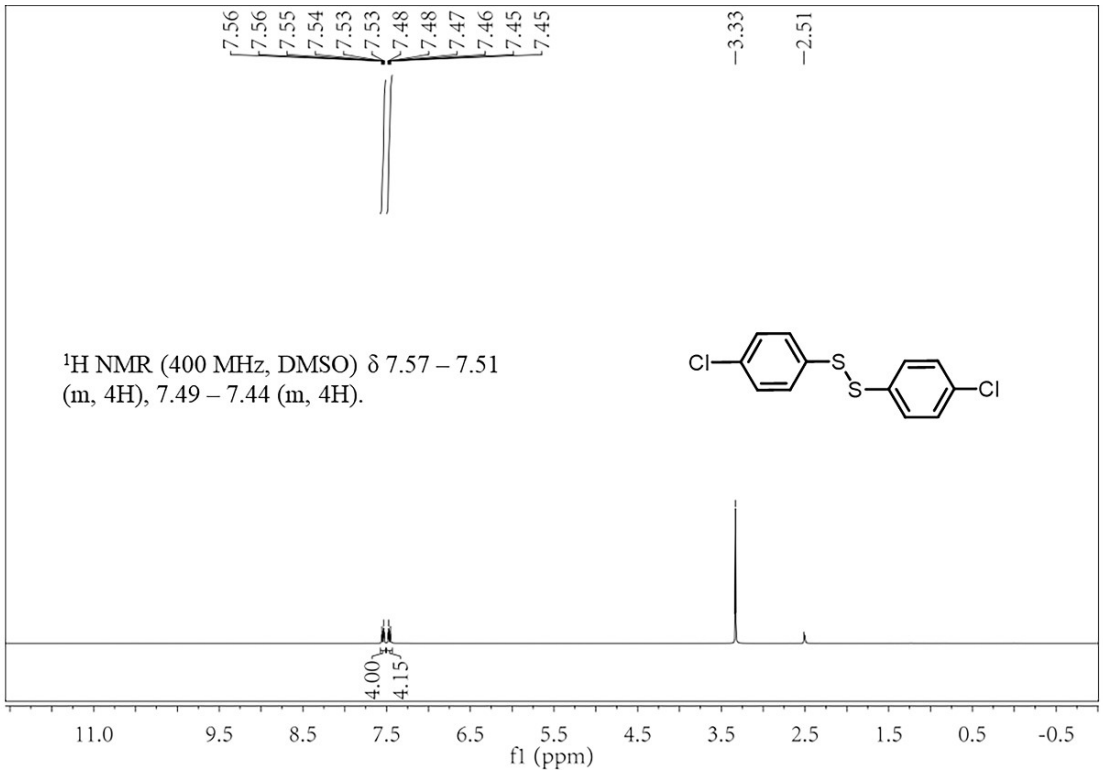

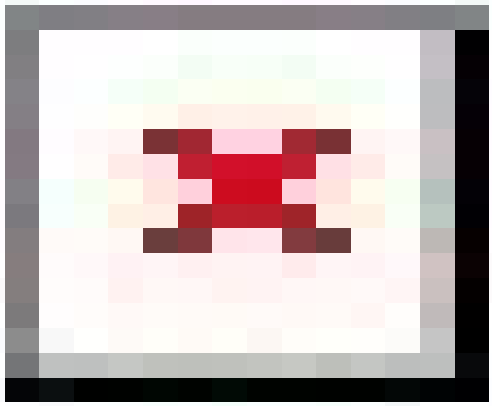

Fig. S9. ^{1}H NMR and ^{13}C NMR spectrum of 4,4 '- Dichlorodiphenyl disulfide.

2,2 '- Dichlorodiphenyl disulfide

^{1}H NMR (400 MHz, $CDCl_3$) δ 7.55 (dd, *J* = 7.9, 1.4 Hz, 2H), 7.36 (dd, *J* = 7.8, 1.1 Hz, 2H), 7.18 (dtd, *J* = 25.1, 7.5, 1.3 Hz, 4H).

^{13}C NMR (101 MHz, $CDCl_3$) δ 134.42, 131.92, 129.74, 127.84, 127.59, 127.27.

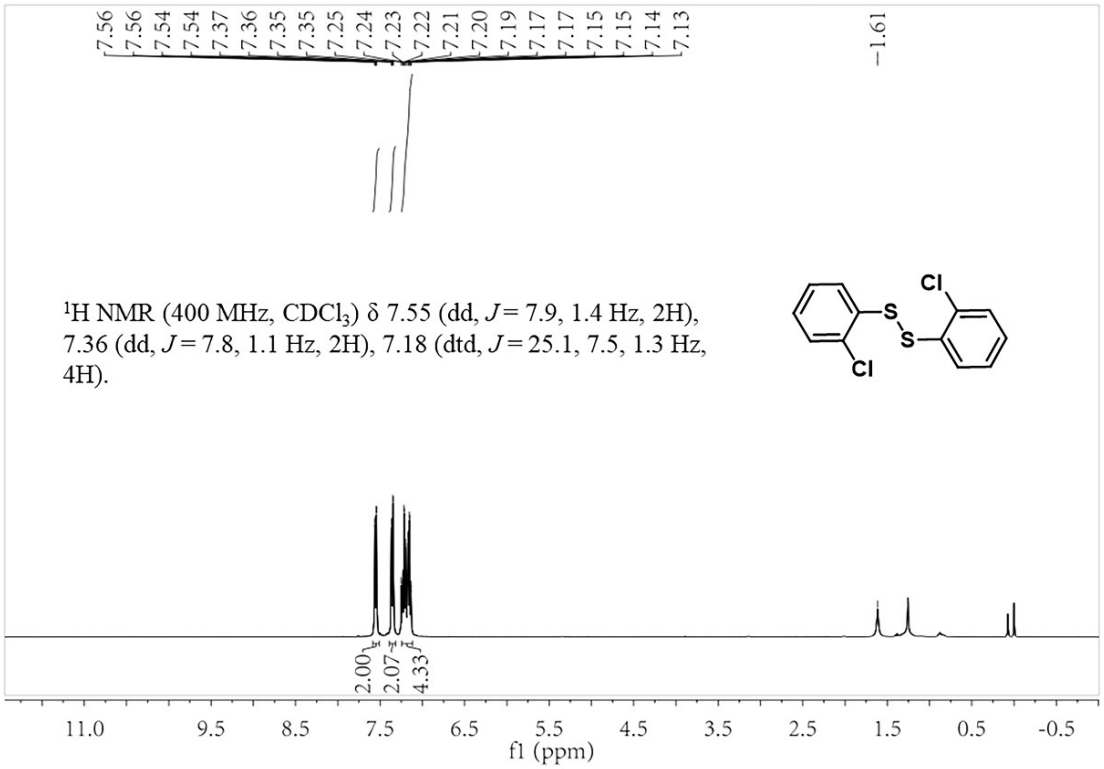

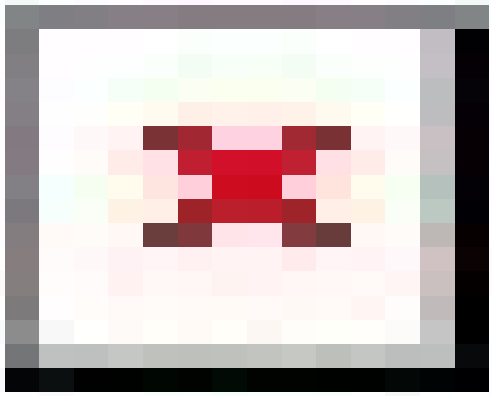

Fig. S10. ^{1}H NMR and ^{13}C NMR spectrum of 2,2 '- Dichlorodiphenyl disulfide.

3,3 '- Dimethyldiphenyl disulfide

^{1}H NMR (400 MHz, $CDCl_3$) δ 7.30 (d, J = 6.6 Hz, 4H), 7.23 – 7.13 (m, 2H), 7.03 (d, J = 7.5 Hz, 2H), 2.32 (s, 6H).

^{13}C NMR (101 MHz, $CDCl_3$) δ 138.92, 136.92, 128.89, 128.03, 128.01, 124.58, 21.38.

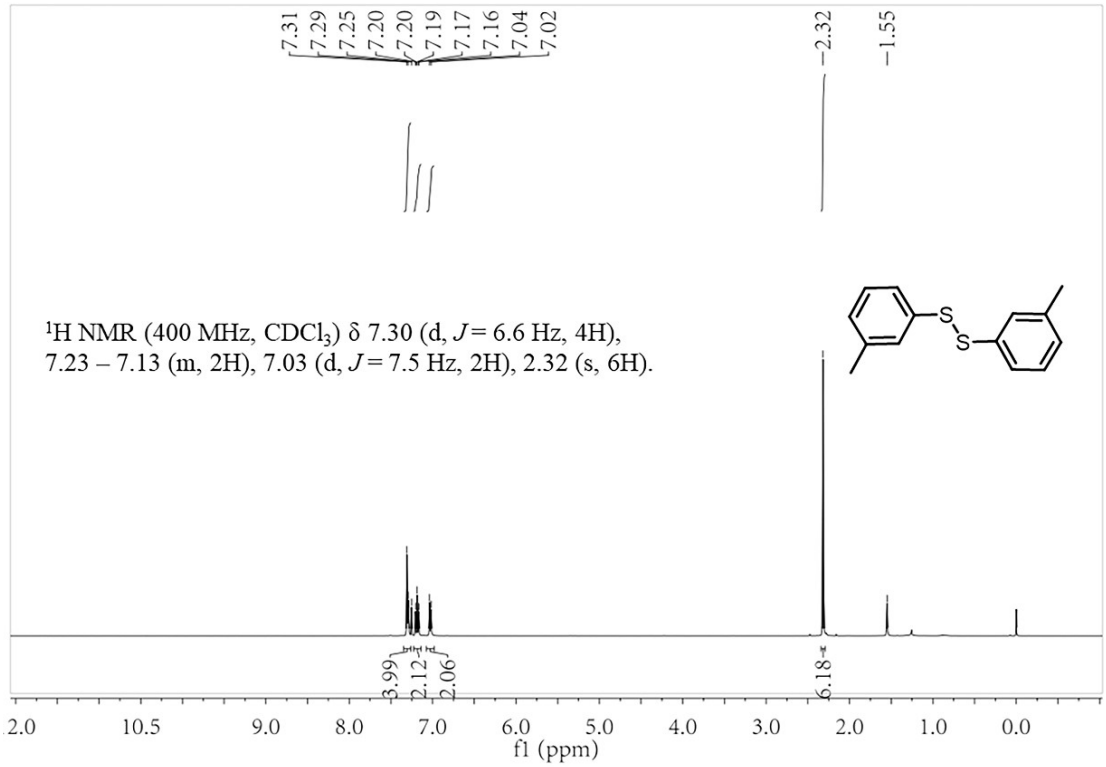

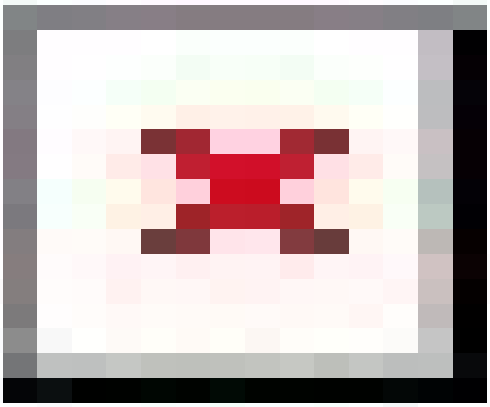

Fig. S11. ^{1}H NMR and ^{13}C NMR spectrum of 3,3 '- Dimethyldiphenyl disulfide.

4,4 '- Dimethyldiphenyl disulfide

^{1}H NMR (400 MHz, $CDCl_3$) δ 7.38 (d, J = 8.2 Hz, 4H), 7.10 (d, J = 8.1 Hz, 4H), 2.31 (s, 6H).

^{13}C NMR (101 MHz, $CDCl_3$) δ 137.45, 133.92, 129.80, 128.56, 21.08.

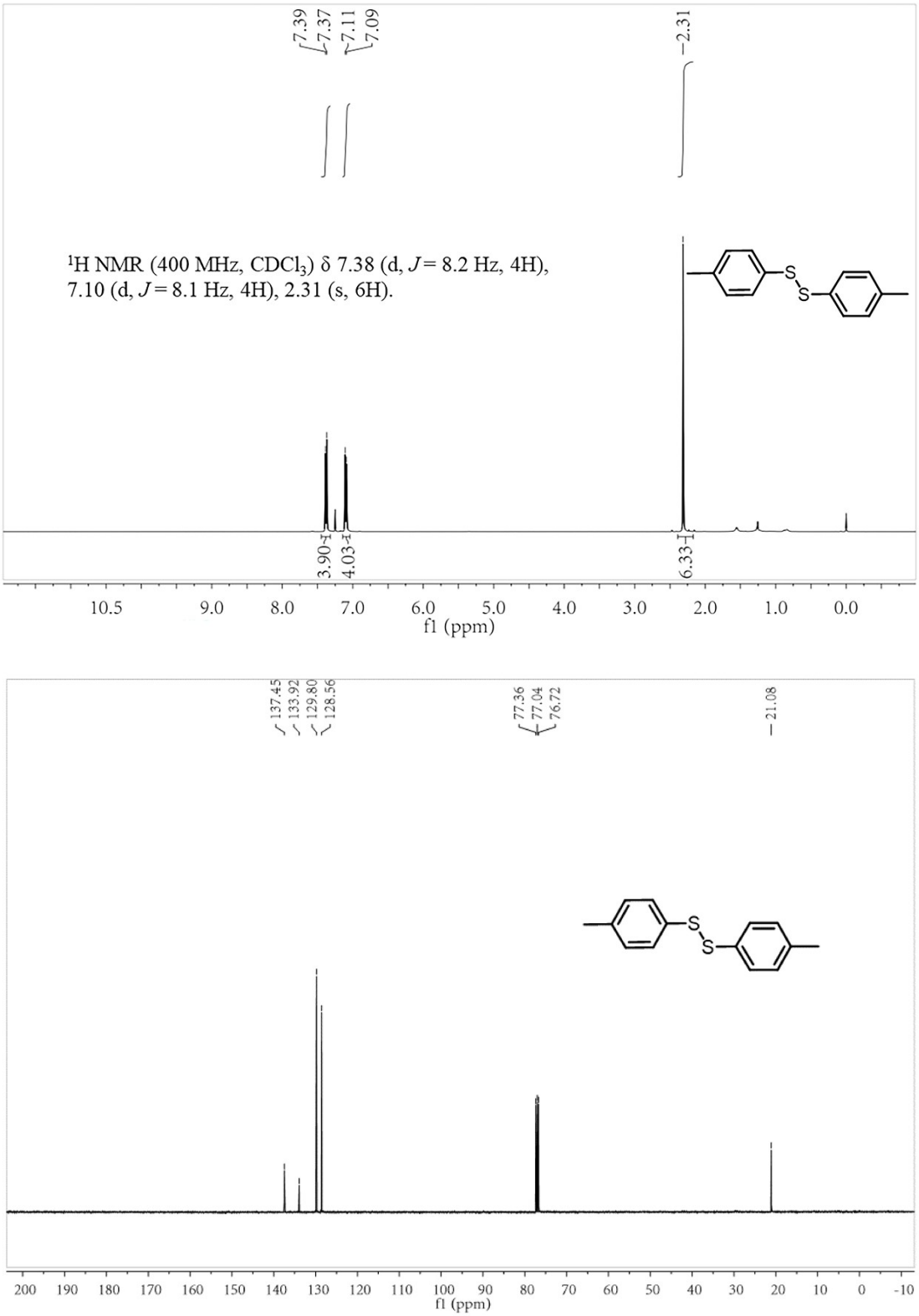

Fig. S12. ^{1}H NMR and ^{13}C NMR spectrum of 4,4 '- Dimethyldiphenyl disulfide.

4,4 - Dihydroxydiphenyl disulfide

^{1}H NMR (400 MHz, $CDCl_3$) δ 7.39 (d, *J* = 8.5 Hz, 4H), 6.83 (d, *J* = 8.5 Hz, 4H), 3.79 (s, 6H).

^{13}C NMR (101 MHz, $CDCl_3$) δ 159.92, 132.67, 128.45, 114.62, 55.38.

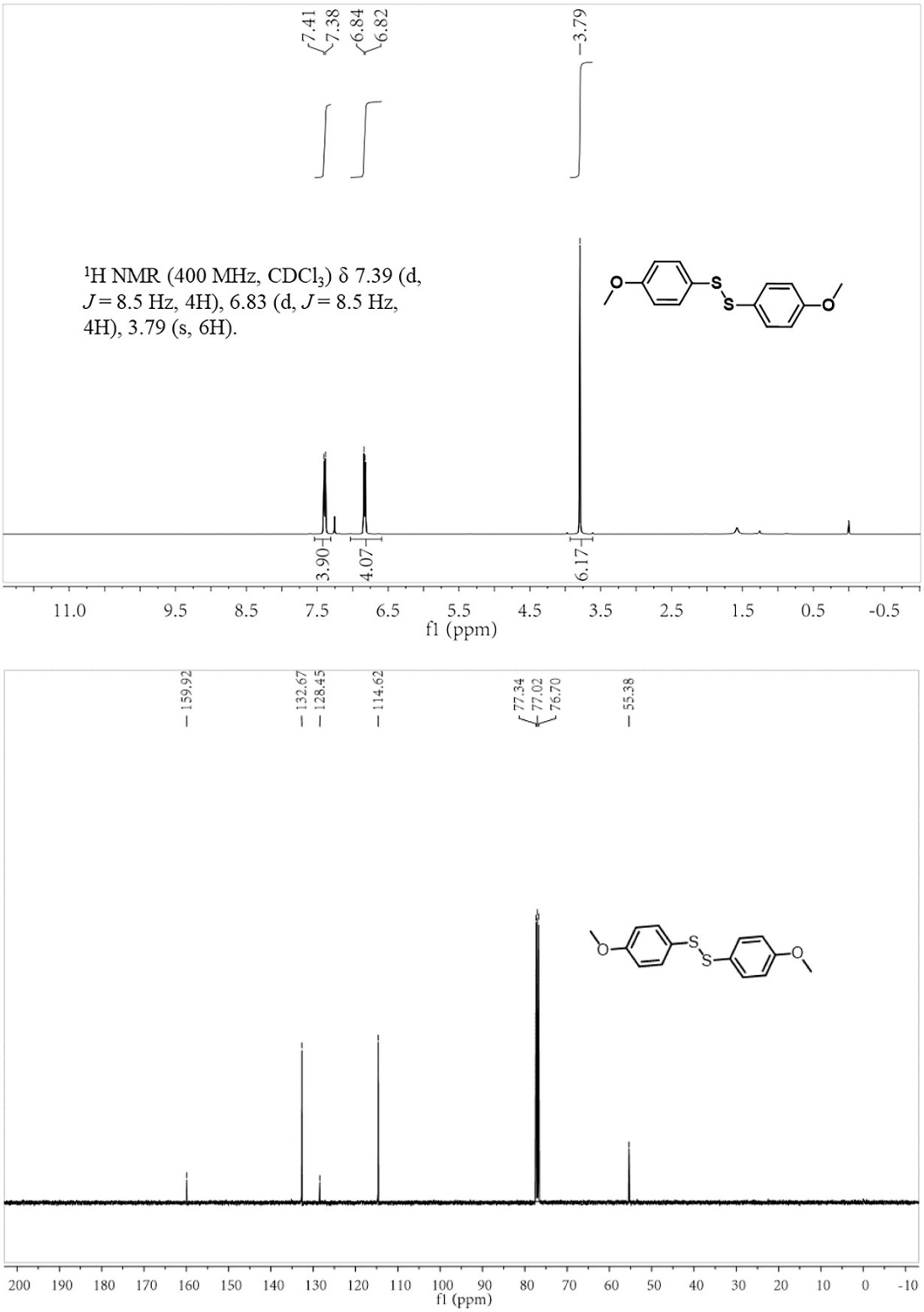

Fig. S13. ^{1}H NMR and ^{13}C NMR spectrum of 4,4 - Dihydroxydiphenyl disulfide.

Benzyl disulfide

^{1}H NMR (400 MHz, $CDCl_3$) δ 7.35 – 7.21 (m, 10H), 3.59 (s, 4H).

^{13}C NMR (101 MHz, $CDCl_3$) δ 137.39, 129.43, 128.50, 127.44, 43.32.

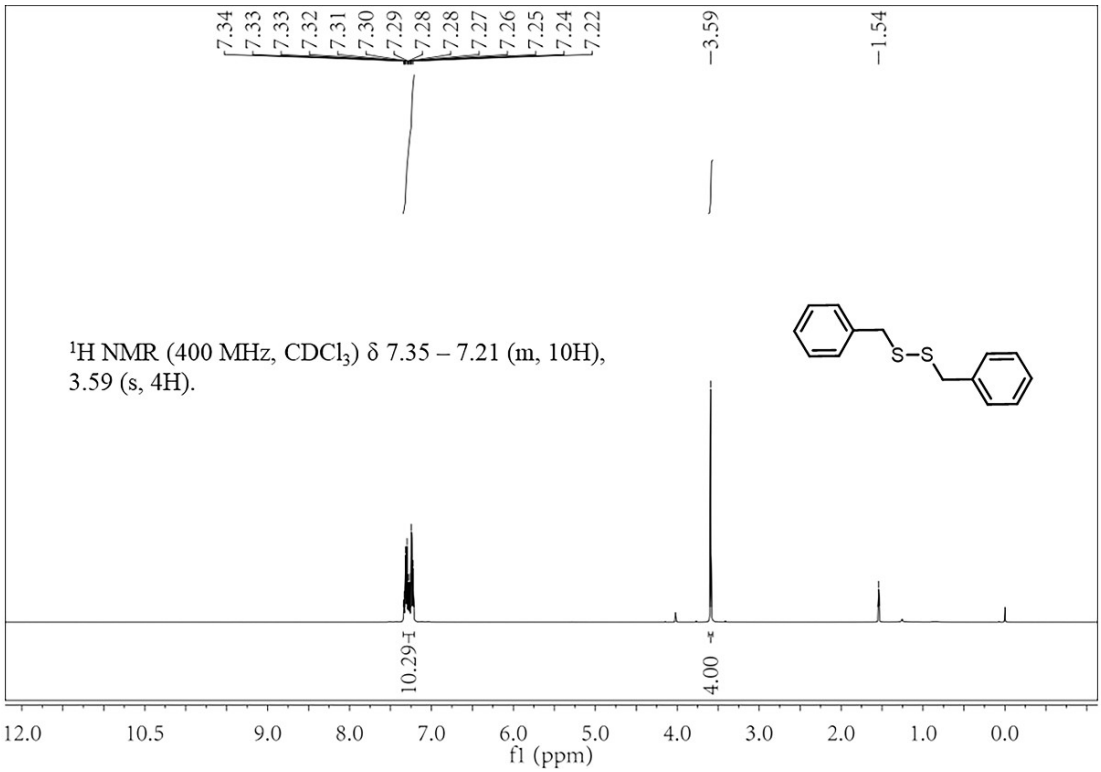

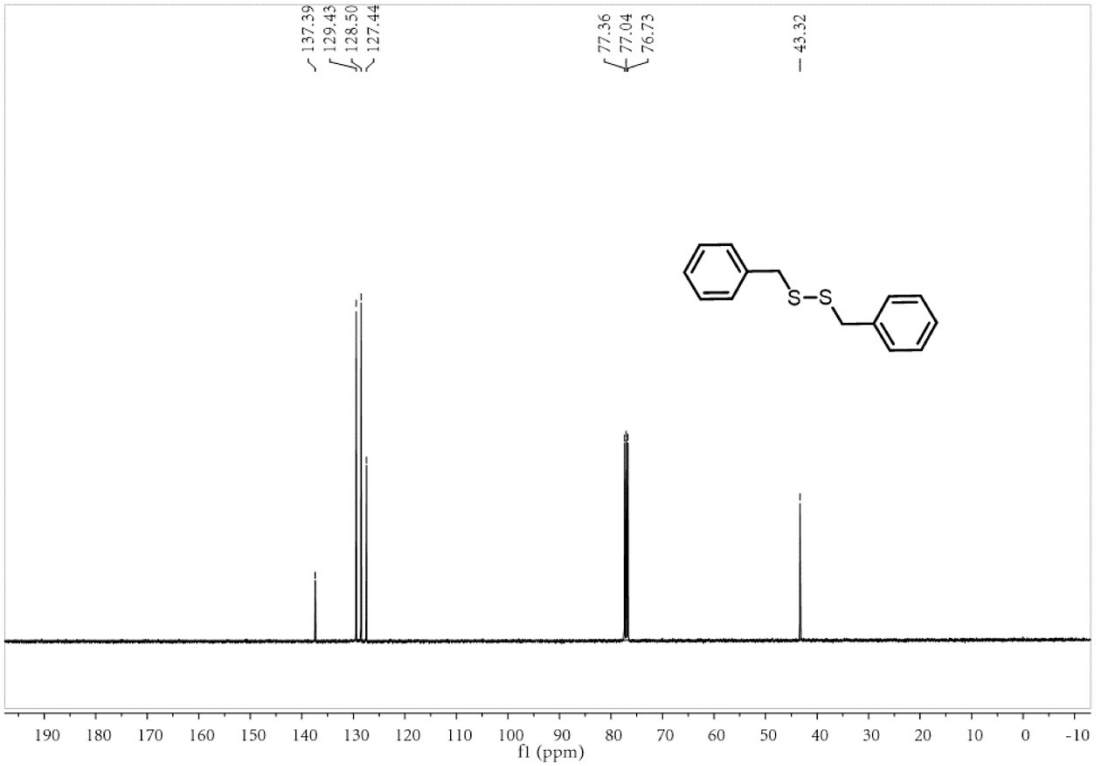

Fig. S14. ^{1}H NMR and ^{13}C NMR spectrum of benzyl disulfide.

2-phenyl-benzimidazol

^{1}H NMR (400 MHz, DMSO) δ 12.90 (s, 1H), 8.19 (d, *J* = 7.3 Hz, 2H), 7.67 – 7.45 (m, 5H), 7.22 (dd, *J* = 5.7, 3.0 Hz, 2H).

^{13}C NMR (101 MHz, $CDCl_3$) δ 130.26, 129.11, 126.54, 123.05.

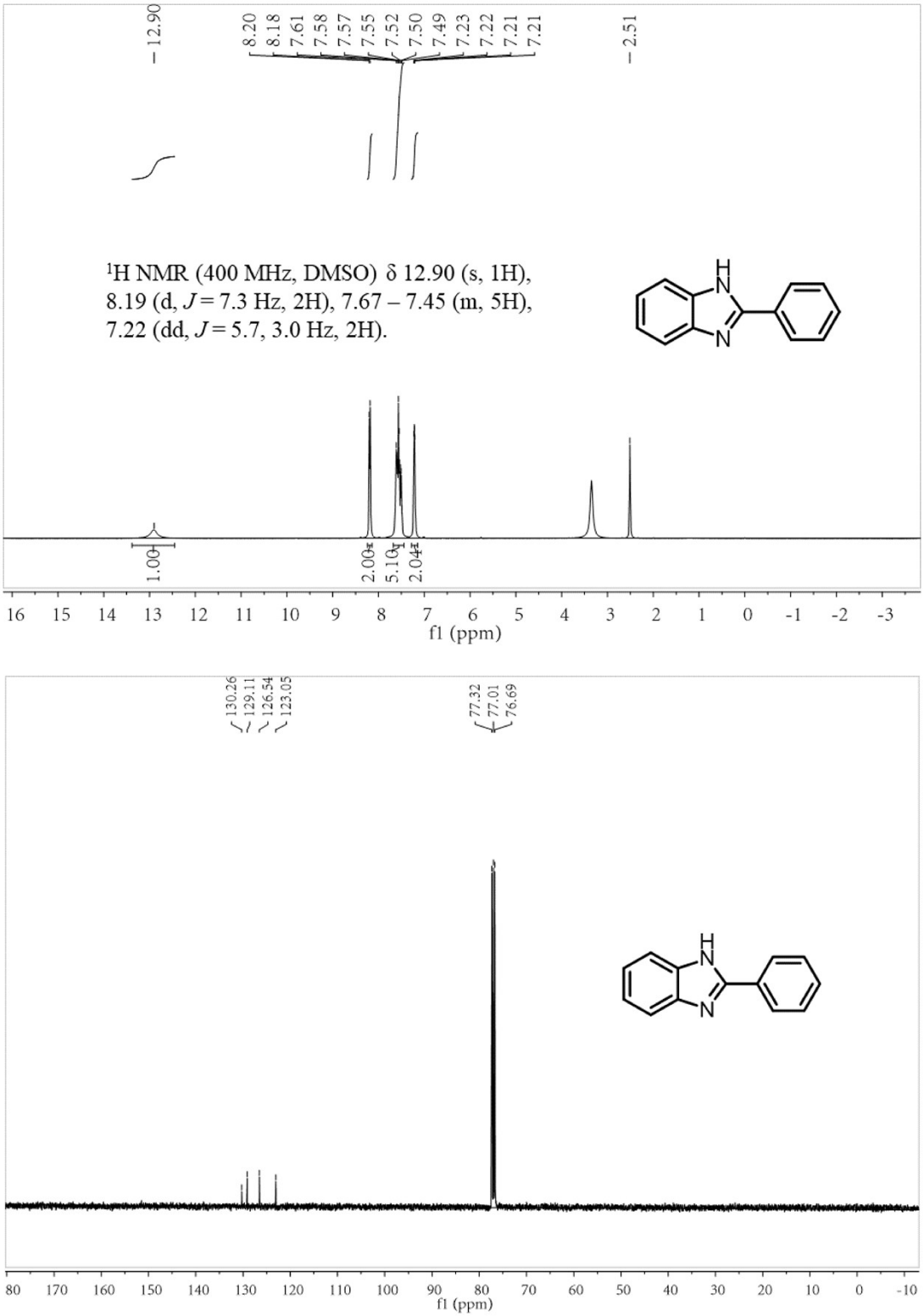

Fig. S15. ^{1}H NMR and ^{13}C NMR spectrum of 2-phenyl-benzimidazol.

2-(4-bromophenyl)- 1H-benzimidazole

^{1}H NMR (400 MHz, DMSO) δ 13.07 (s, 1H), 8.26 (d, *J* = 8.5 Hz, 2H), 7.79 – 7.56 (m, 4H), 7.36 – 7.20 (m, 2H).

^{13}C NMR (101 MHz, $CDCl_3$) δ 155.92, 132.00, 129.98, 128.06, 118.51, 117.06, 115.54.

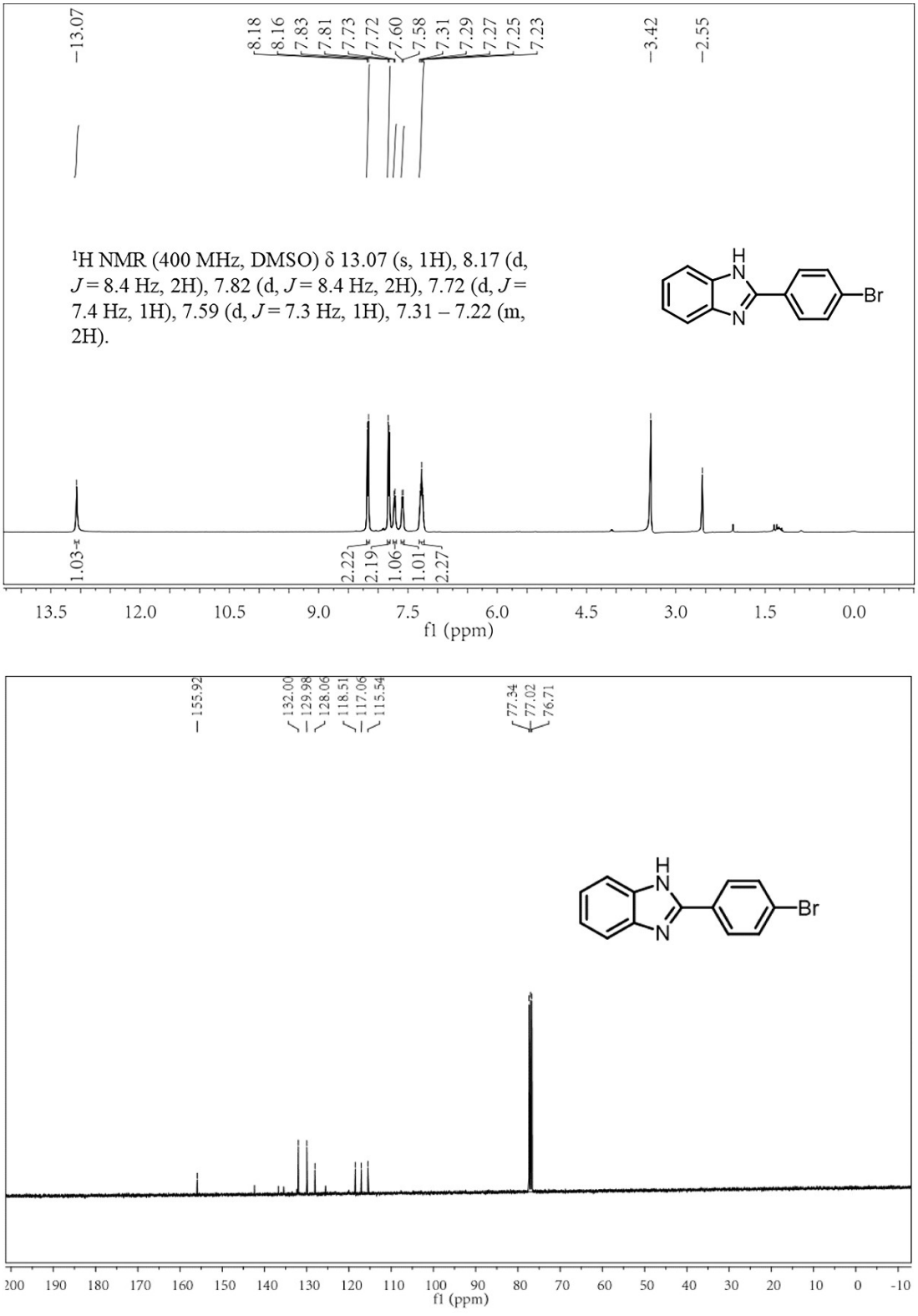

Fig. S16. ^{1}H NMR spectrum of 2-(4-bromophenyl)- 1H-benzimidazole.

2-(4-chlorophenyl)-1H-benzimidazole

^{1}H NMR (400 MHz, DMSO) δ 13.07 (s, 1H), 8.26 (d, *J* = 8.5 Hz, 2H), 7.79 – 7.56 (m, 4H), 7.36 – 7.20 (m, 2H).

^{13}C NMR (101 MHz, DMSO) δ 150.61, 134.94, 129.53, 128.59, 122.77.

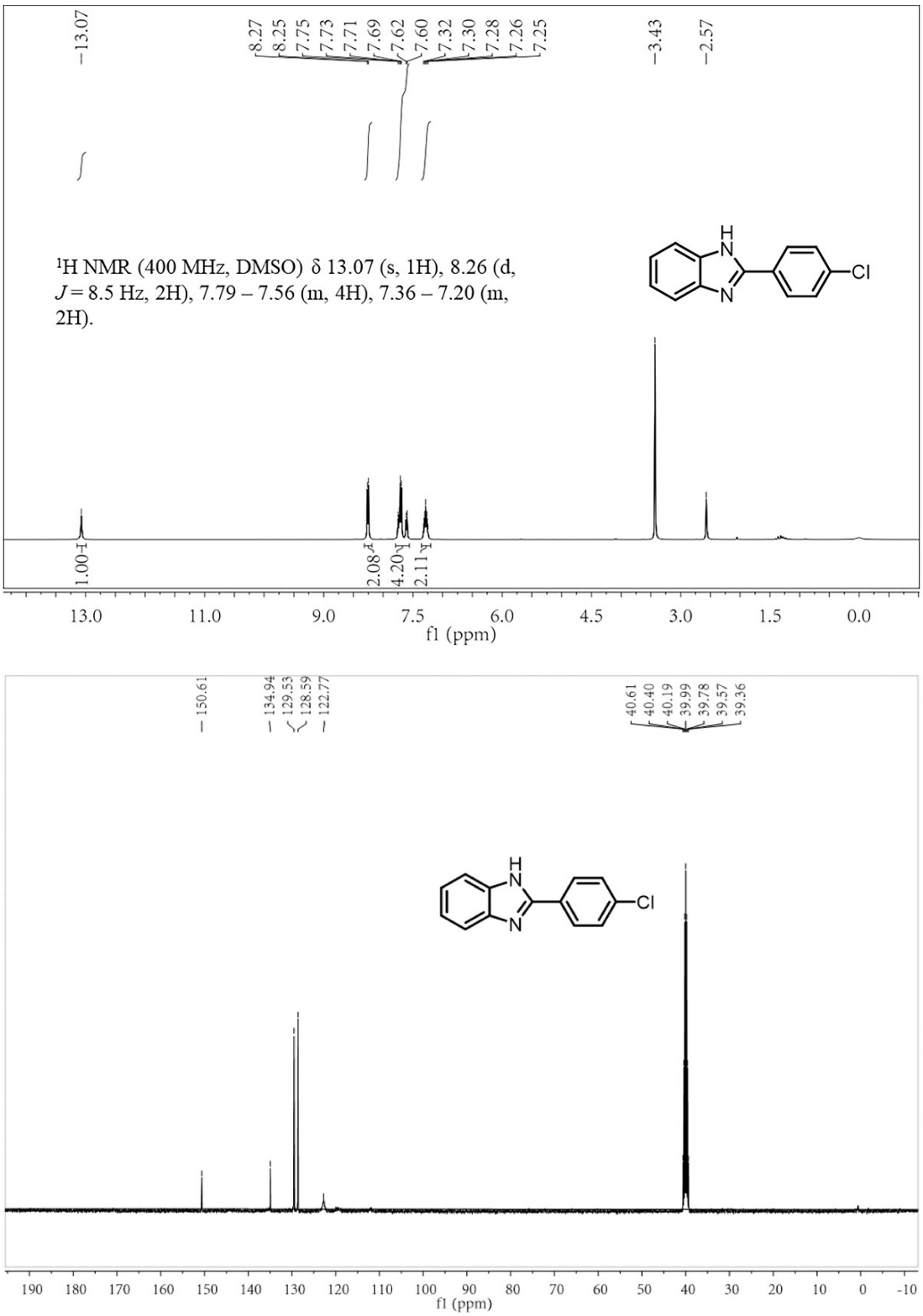

Fig. S17. ^{1}H NMR and ^{13}C NMR spectrum of 2-(4-chlorophenyl)-1H-benzimidazole.

2-(4-methylphenyl)-1H-benzimidazole

^{1}H NMR (400 MHz, DMSO) δ 12.76 (s, 1H), 8.00 (d, *J* = 8.1 Hz, 2H), 7.51 (s, 2H), 7.28 (d, *J* = 8.0 Hz, 2H), 7.12 (dd, *J* = 5.7, 2.8 Hz, 2H), 2.30 (s, 3H).

^{13}C NMR (101 MHz, DMSO) δ 151.83, 140.01, 129.97, 127.91, 126.85, 122.40, 21.44.

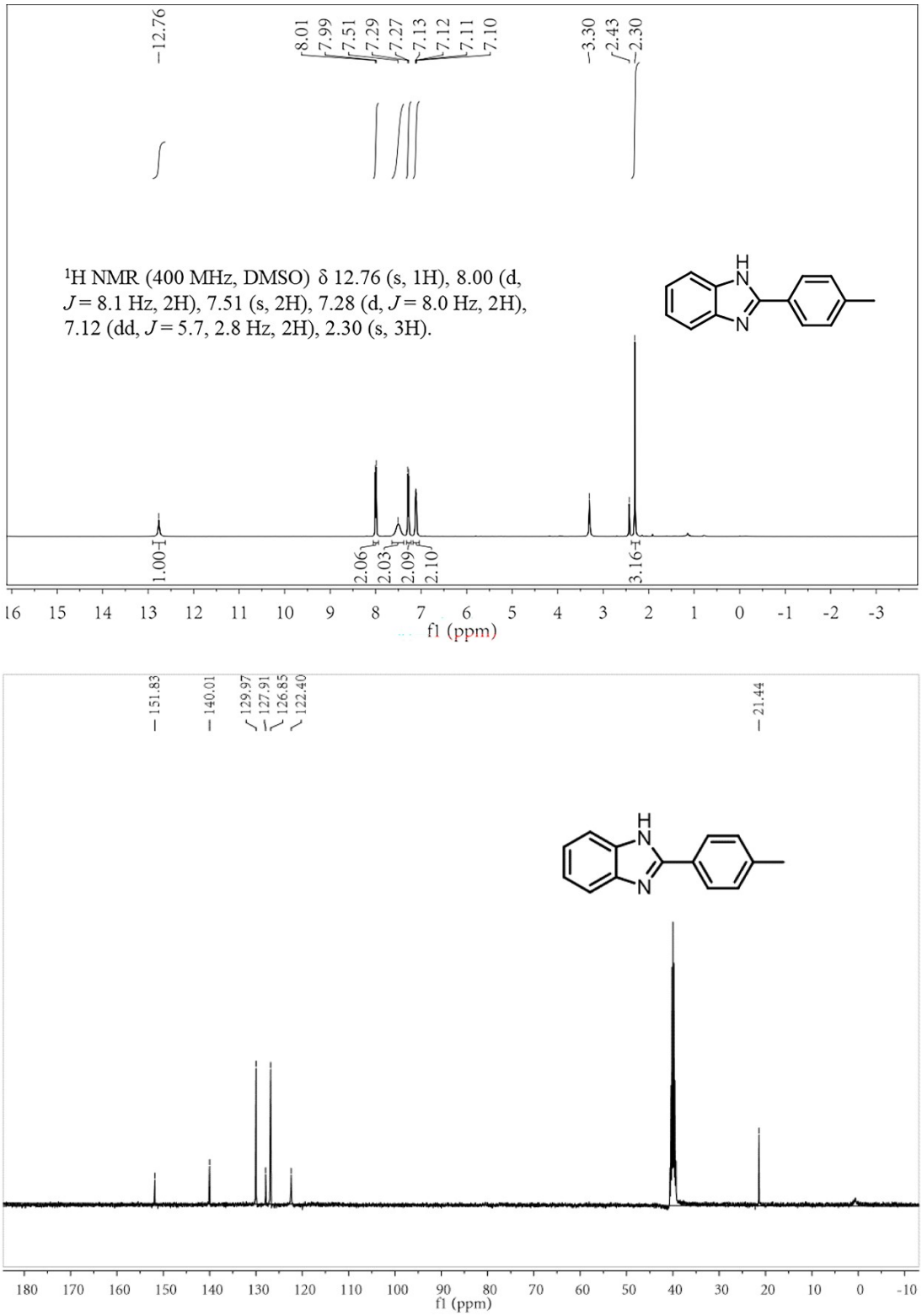

Fig. S18. ^{1}H NMR and ^{13}C NMR spectrum of 2-(4-methylphenyl)-1H-benzimidazole.

2-(2-Thienyl)-1H-benzimidazole

^{1}H NMR (400 MHz, DMSO) δ 13.01 (s, 1H), 7.89 (dd, *J* = 3.6, 1.0 Hz, 1H), 7.78 (dd, *J* = 5.0, 1.0 Hz, 1H), 7.55 (d, *J* = 7.3 Hz, 1H), 7.33 – 7.17 (m, 3H).

^{13}C NMR (101 MHz, DMSO) δ 147.49, 134.18, 129.20, 128.73, 127.14.

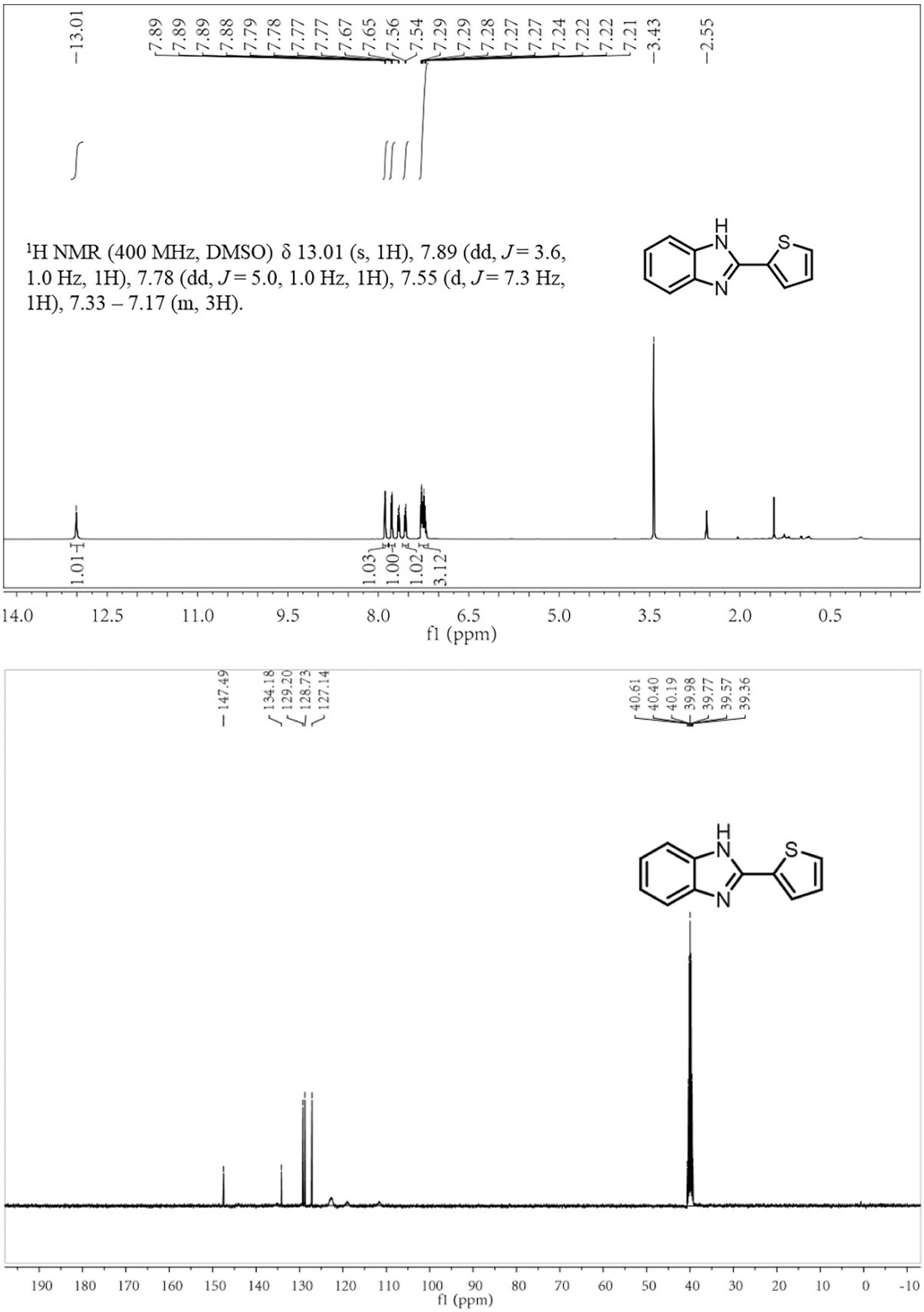

Fig. S19. ^{1}H NMR and ^{13}C NMR spectrum of 2-(2-Thienyl)-1H-benzimidazole.

4-(1H-benzoimidazol-2-yl)-phenol

^{1}H NMR (400 MHz, DMSO) δ 12.70 (s, 1H), 10.04 (s, 1H), 8.06 (d, *J* = 8.6 Hz, 2H), 7.59 (dd, *J* = 5.4, 3.1 Hz, 2H), 7.25 – 7.14 (m, 2H), 6.97 (d, *J* = 8.6 Hz, 2H).

^{13}C NMR (101 MHz, DMSO) δ 159.57, 152.22, 128.60, 122.07, 121.58, 116.13.

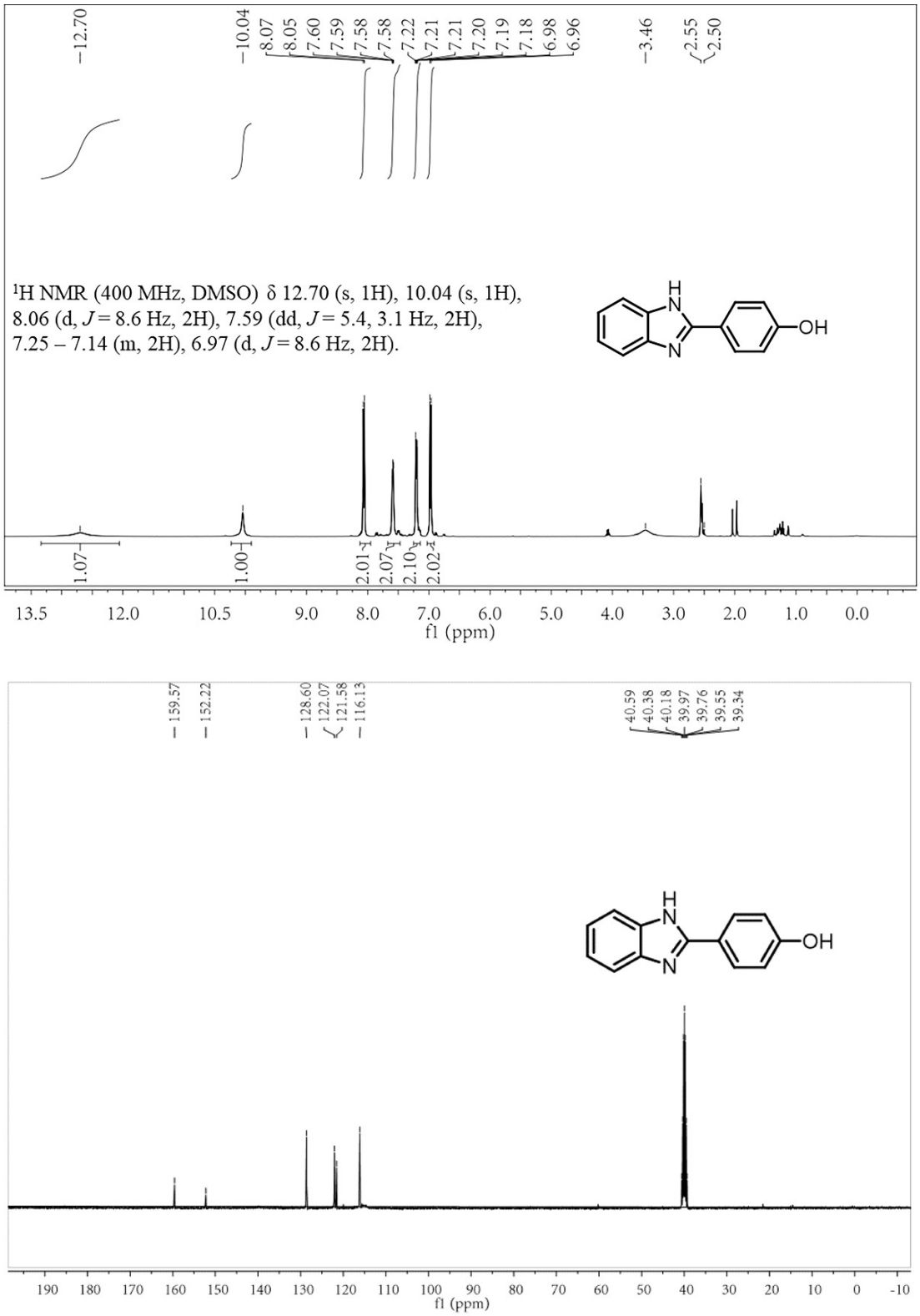

Fig. S20. ^{1}H NMR and ^{13}C NMR spectrum of 4-(1H-benzoimidazol-2-yl)-phenol.

2-(4-Fluorophenyl)-1H-benzimidazole

^{1}H NMR (400 MHz, DMSO) δ 12.99 (s, 1H), 8.26 (dd, *J* = 8.2, 5.6 Hz, 2H), 7.63 (s, 2H), 7.44 (t, *J* = 8.7 Hz, 2H), 7.31 – 7.15 (m, 2H).

^{13}C NMR (101 MHz, MeOD) δ 165.22, 162.71, 151.01, 138.76, 128.68, 122.58, 115.79, 115.57, 114.46.

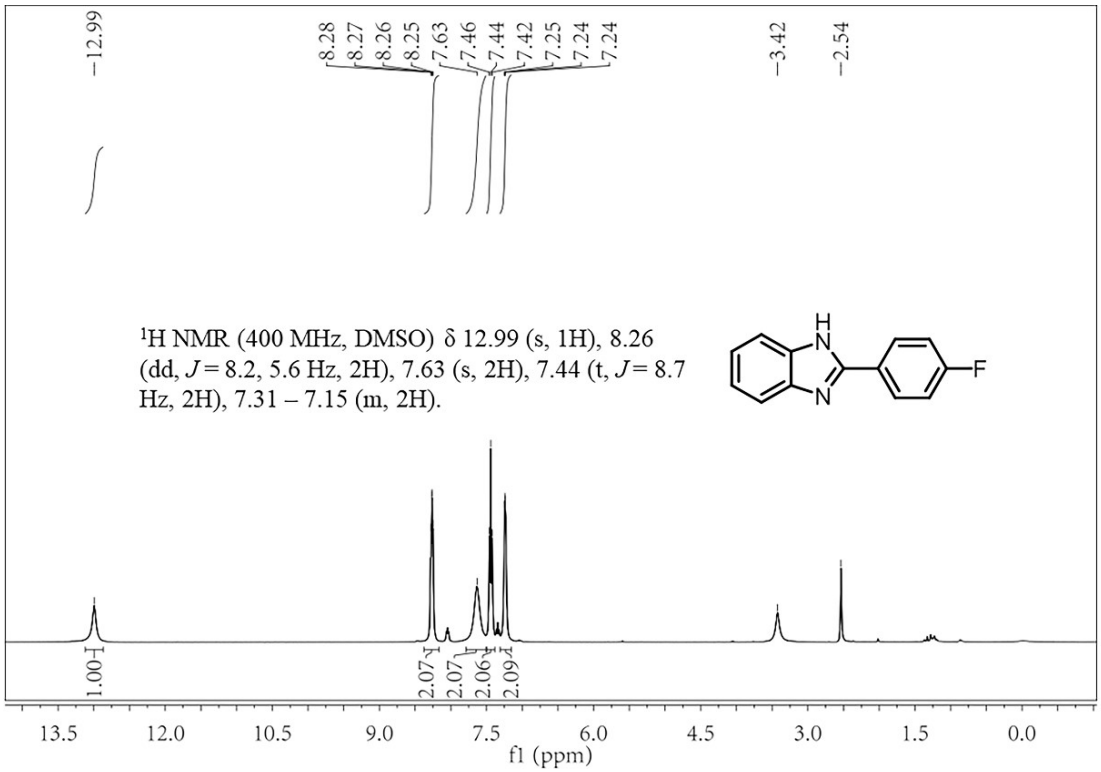

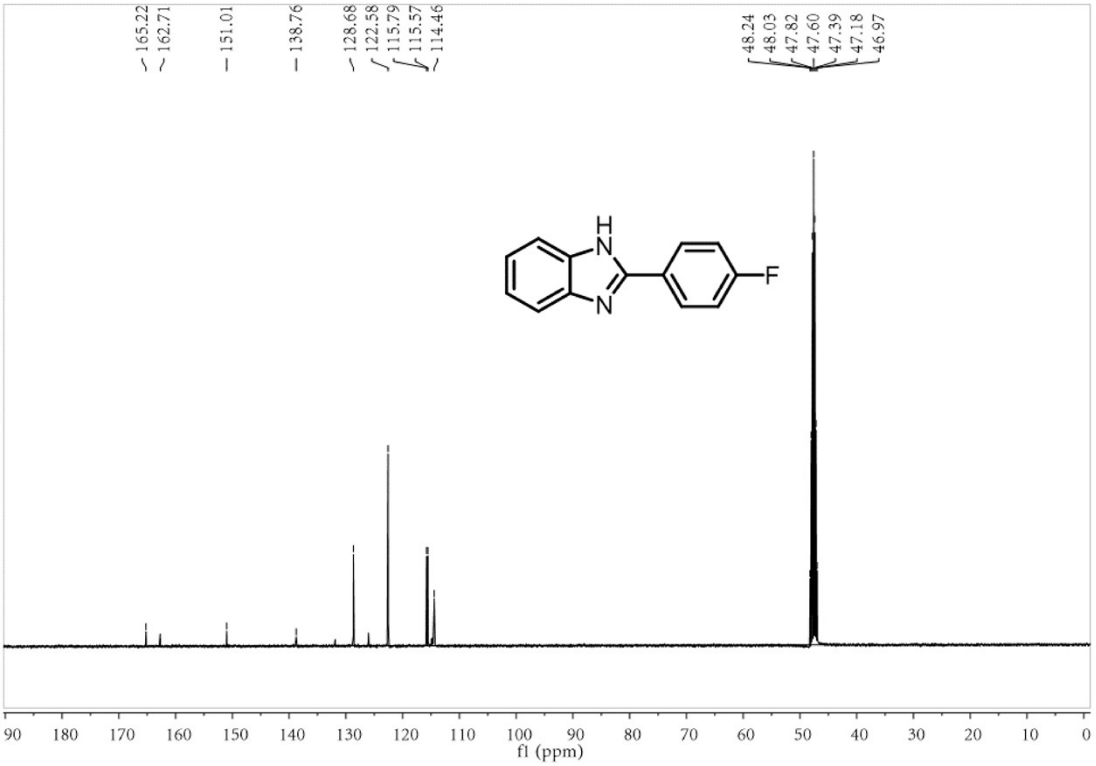

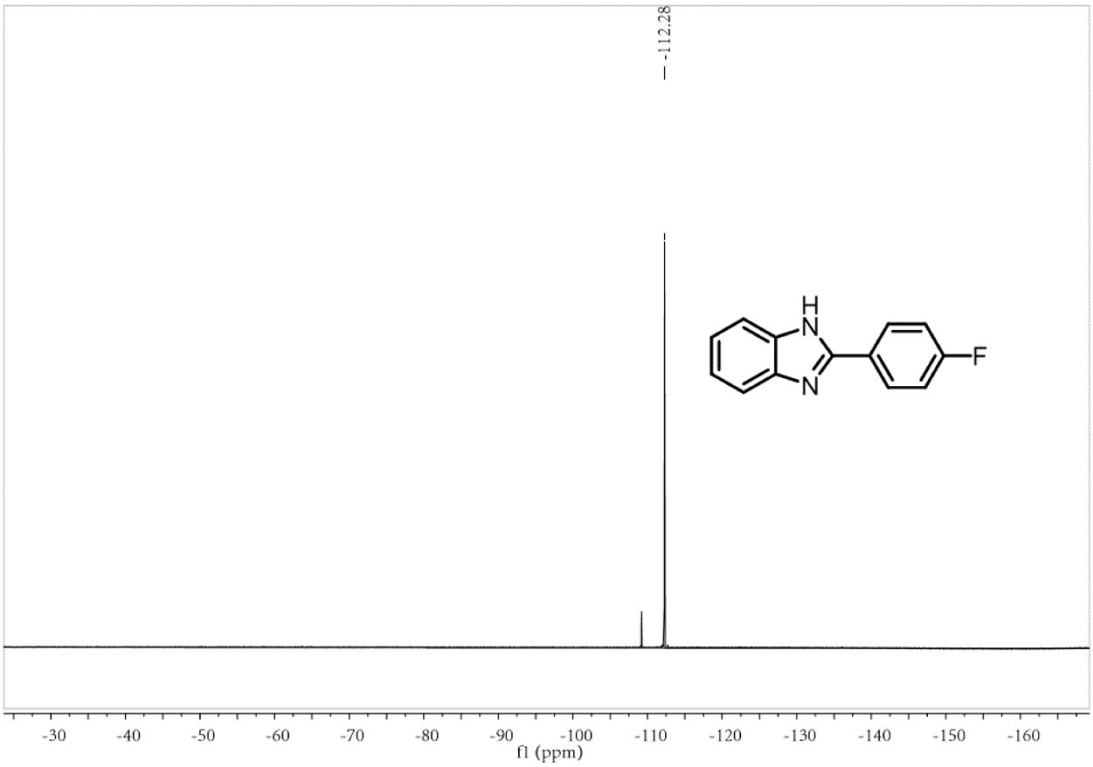

Fig. S21. ^{1}H NMR, ^{13}C NMR and ^{19}F NMR spectrum of 2-(4-Fluorophenyl)-1H-benzimidazole.

2-(2-nitro-5-chlorophenyl)-1H-benzimidazole

^{1}H NMR (400 MHz, DMSO) δ 13.22 (s, 1H), 8.15 (dd, *J* = 16.3, 5.4 Hz, 2H), 7.90 (dd, *J* = 8.6, 2.1 Hz, 1H), 7.69 (s, 2H), 7.32 (s, 2H).

^{13}C NMR (101 MHz, MeOD) δ 147.01, 138.82, 131.49, 130.76, 127.14, 126.32.

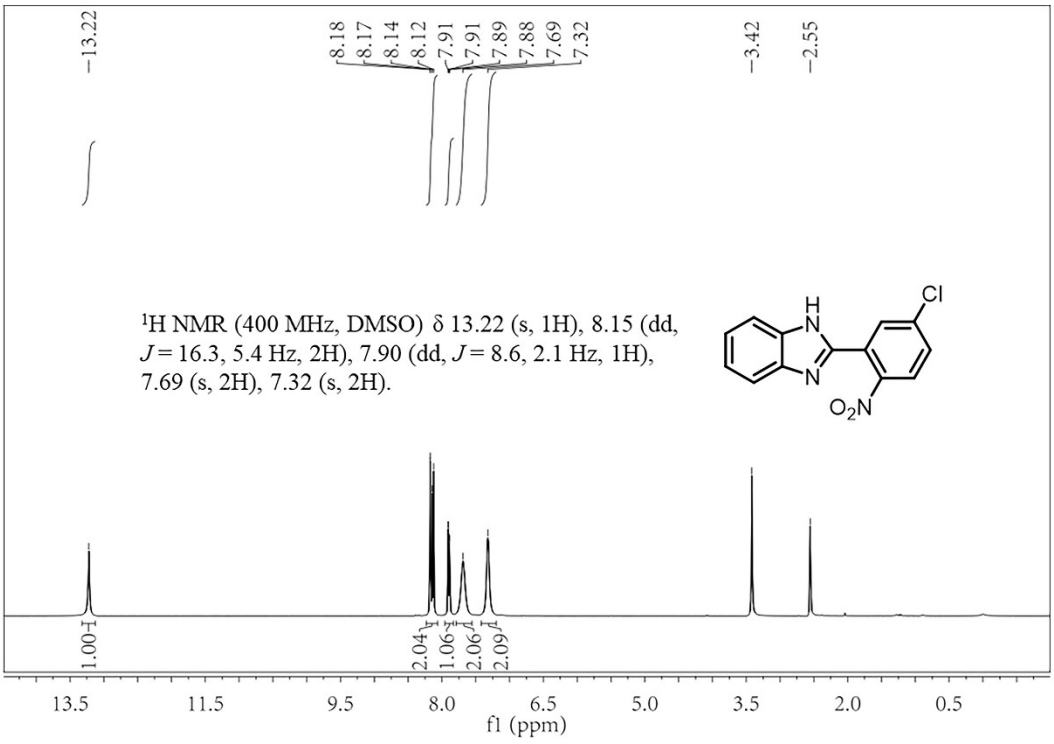

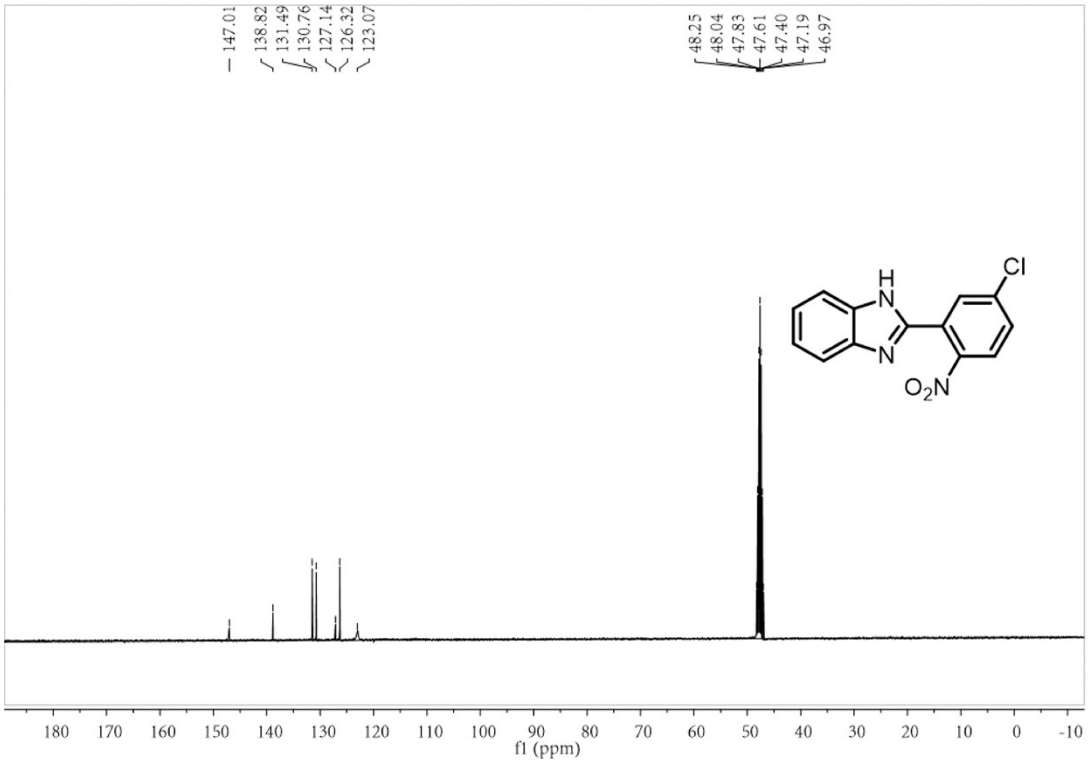

Fig. S22. ^{1}H NMR and ^{13}C NMR spectrum of 2-(2-nitro-5-chlorophenyl)-1H-benzimidazole.

2-(3-Chlorophenyl)-1H-benziMidazole

^{1}H NMR (400 MHz, DMSO) δ 13.11 (s, 1H), 8.29 (d, *J* = 1.7 Hz, 1H), 8.20 (dt, *J* = 7.3, 1.6 Hz, 1H), 7.66 (ddd, *J* = 21.9, 10.2, 7.1 Hz, 4H), 7.35 – 7.20 (m, 2H).

^{13}C NMR (101 MHz, MeOD) δ 150.34, 134.77, 131.53, 130.32, 129.72, 126.28, 124.61, 122.83.

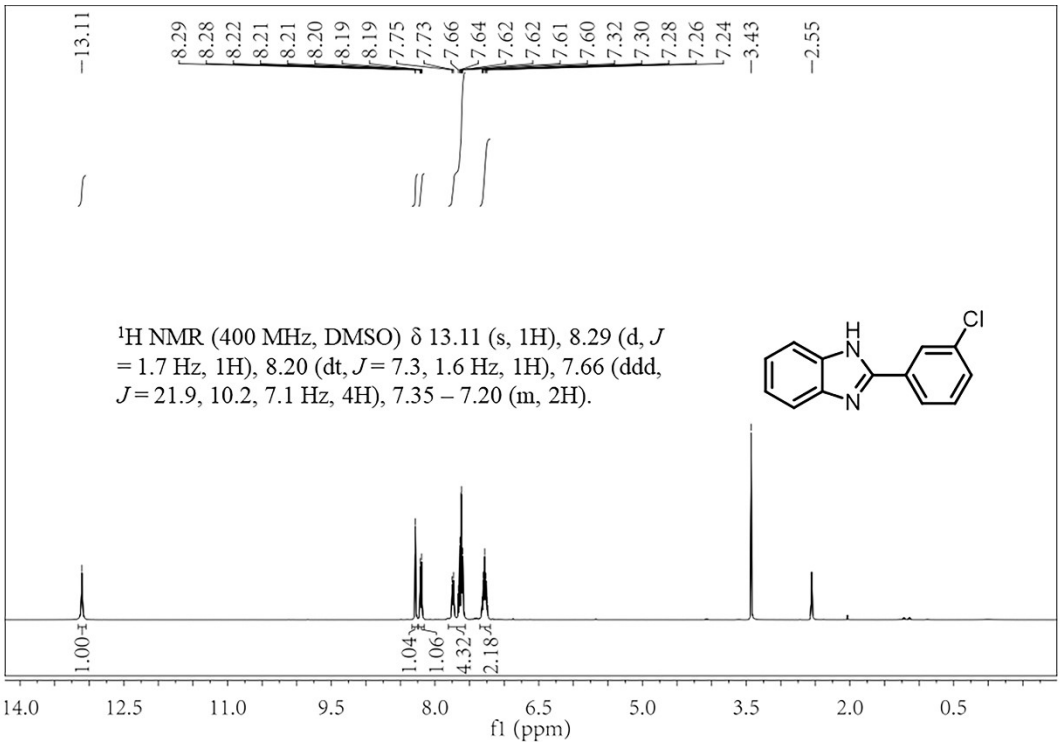

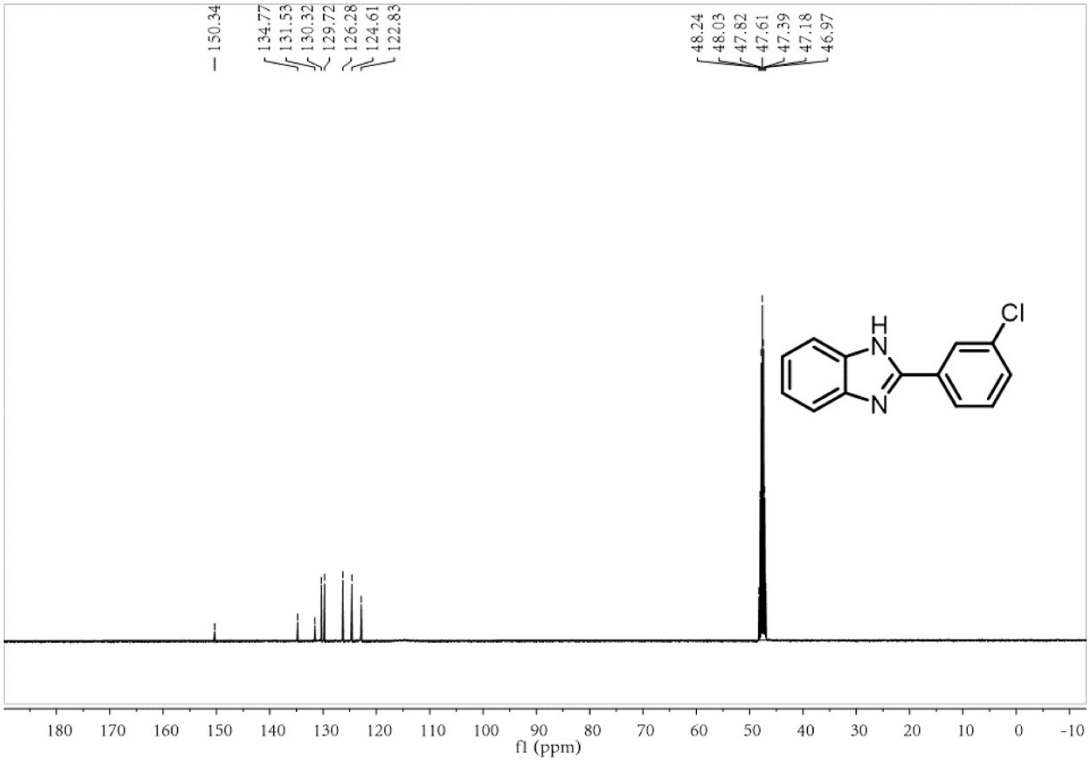

Fig. S23. ^{1}H NMR and ^{13}C NMR spectrum of 2-(3-Chlorophenyl)-1H-benziMidazole.

References

1. Corma, A.; Ródenas, T.; Sabater, M. J., Aerobic oxidation of thiols to disulfides by heterogeneous goldcatalysts. *Chem. Sci.* **2012,** *3* (2), 398-404.

2. Sha, Y.; Lin, X.-M.; Niklas, J.; Poluektov, O. G.; Diroll, B. T.; Lin, Y.; Wen, J.; Hood, Z. D.; Lei, A.; Shevchenko, E. V., Insights into the extraction of photogenerated holes from CdSe/CdS nanorods for oxidative organic catalysis. *J. Mater. Chem. A* **2021,** *9* (21), 12690-12699.

3. Huang, X.; Lu, Y.; Mao, G.; Yin, S.; Long, B.; Deng, G.-J.; Ali, A.; Song, T., Polarization engineering of porous organic polymers for superior photocatalytic synthesis of disulfides and CO2 reduction. *J. Mater. Chem. A* **2022,** *10* (45), 24147-24155.

4. Spiliopoulou, N.; Kokotos, C. G., Photochemical metal-free aerobic oxidation of thiols to disulfides. *Green Chem.* **2021,** *23* (1), 546-551.